Spectrum Occupancy Investigation: Measurements in South Africa

S.D. Barnes*, P.A. Jansen van Vuuren, B.T. Maharaj

Department of Electrical, Electronic and Computer Engineering, University of Pretoria, Pretoria, 0002, South Africa

Abstract

Regulatory bodies have predicted an impending shortage in commercial radio frequency spectrum in the near future. However, due to outdated regulatory practices, many of these bands are in fact inefficiently underutilised. Spectrum measurement campaigns have be carried out around the world to determine the extent to which this is true. However, there still seems to be a lack of knowledge regarding spectrum occupancy in South Africa. A spectrum measurement system was thus designed and employed to measure the spectrum occupancy of the ultra-high frequency (UHF), global system for mobile communications (GSM) 900 MHz and GSM 1800 MHz bands through a measurement campaign in the Hatfield area of Pretoria, South Africa. A method for determining spectrum occupancy, from raw spectrum measurements, has been described and used to calculate the average spectrum occupancy of these bands. Occupancy in the UHF band was found to be fairly constant at approximately only 20%. While the maximum occupancy of the GSM 900 MHz band was calculated to be much higher at approximately 92% and that of the GSM 1800 band to be approximately 40%. However, the GSM 900 MHz and 1800 MHz bands did exhibit fluctuations in occupancy of between 10% and 20% respectively according to the time of day. Slight variations in occupancy of between 1% and 3% were also evident over the days of the week. These results are placed into context by a comparison with the findings of various other measurement campaigns from around the world. When compared, occupancy was generally found to be lower in the UHF bands but higher in the mobile bands.

Keywords:

Cognitive radio, Noise floor, Spectrum measurements, Spectrum occupancy, Threshold detection

1. Introduction

The Federal Communications Commission (FCC) of the United States of America (USA) and various other regulatory bodies worldwide have found that in many frequency bands the radio frequency spectrum is currently underutilised. This is in spite of recent trends towards an increase in the demand for wireless connectivity [1]. With most of the useful radio spectrum already allocated, it is becoming difficult to find vacant bands to either deploy new services or enhance existing ones. Thus it seems that useful radio frequency spectrum is gradually becoming a more scarce resource [2]. This has led to the development of cognitive radio technologies, which rely heavily on understanding the spectrum occupancy dynamics of available radio resources [3, 4].

Various measurement campaigns have been undertaken in other countries [5, 6, 7, 8, 9, 10, 11, 12, 13, 14, 15], but there is still a general lack of knowledge regarding spectrum occupancy in Africa, and more specifically in South Africa. This research project sought to fill this gap by developing a mobile autonomous system which can be used to

*Corresponding author, Tel.: +27 12 420 2872.
Email address: simonbarnes@ieee.org (S.D. Barnes)

gather spectrum occupancy information for a wide range of frequencies over long periods of time. A modular hardware system and software environment was developed to deliver detailed information about the occupancy of various commercially utilised South African frequency bands. These included the ultra-high frequency (UHF) and global system for mobile communications (GSM) bands. Measurements were thus taken from the following bands,

- UHF (470 MHz - 854 MHz),
- GSM 900 downlink (935 MHz - 960 MHz), and
- GSM 1800 downlink (1805 MHz - 1880 MHz).

Data was collected from a six week long measurement campaign in the Hatfield area of Pretoria, South Africa [16]. The measurement site (GPS Co-ordinates: $S25^\circ\ 45'\ 11''$ $E28^\circ\ 13'\ 42''$) was situated on the Hatfield campus of the University of Pretoria, which is located in a typical urban area with a large student population density. The surrounding area is predominantly characterised by schools, office blocks, shops and student accommodation. The design and configuration of the measurement campaign is described in this article.

A technique for extracting the information bearing component from the noise component of a measured signal, described as the maximum normal fit (MNF) method, is described and used to calculate spectrum occupancy. Detailed information pertaining to the calculated occupancy of the measured bands is then presented and compared to the findings of various other measurement campaigns.

2. Measurement system

In this section the design and configuration of the measurement system is presented. The physical measurement configuration is illustrated in Fig. 1.

2.1. Hardware subsystem

The hardware configuration of the measurement system is illustrated in Fig. 2 in the form of a functional block diagram. Functional unit (FU) H1 is a wide-band Super-M Ultra base antenna with a frequency range of 25 MHz to 6 GHz capable of receiving both vertically and horizontally polarized signals. The main hardware components of the receiver system are housed within a metal cabinet, FU H2, located on the roof of the Engineering I building of the University of Pretoria. This cabinet houses FU H2.1, a low noise amplifier (LNA) with an operating range of 50

Figure 1: Physical spectrum measurement system.

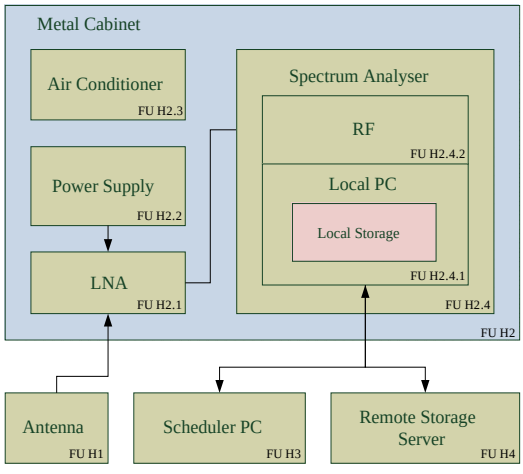

Figure 2: Hardware component functional block diagram of spectrum sensing system.

MHz to 3 GHz (operation at higher frequencies is possible, but at a lower gain), FU H2.2, a regulated 5V DC power supply for powering the LNA, FU H2.3, a custom built air conditioning unit and a spectrum analyser (SA), FU H2.4.

Although physically housed within the same enclosure, the SA FU H2.4, was split into two functional hardware units: a local PC that houses device controlling software, FU H2.4.1, and the radio frequency (RF) component of the device, FU H2.4.2. A temporary storage space is available on the local PC, FU2.4.1.1. FU H1 is connected to FU H2.1 via 10 meters of rugged low loss LMR 600 coaxial cable. FU H2.1 is in turn connected to FU H2.4.2 via a Sucoflex 100 coaxial cable. An Ethernet connection provides the interface between FU H2.4 and two other functional hardware components: FU H3, a remote PC that runs the remote scheduling software and FU H4, a backup and storage server for remote storage and backup of the actual spectrum measurement data. FU H3 and FU H4 were located in an office in the Engineering II building of the University of Pretoria.

2.2. Software description

The software for the measurement campaign has been divided into three separate applications: interface and control software to locally control the SA, manage data files and report on operational status; remote control software to remotely schedule the scans to be performed and allow for easy access to the system configuration function from a remote location; and data backup software to securely store the result files on the backup server. Each component is illustrated in Fig. 3 as a functional block diagram.

The SA interface and control software package interprets the scan configuration command and configures the SA hardware for the appropriate operation. It then awaits the initiate scan commands from the remote control software. Upon receiving said commands, it begins scanning and saving measured data locally on the SA. The remote control software is responsible for reading a measurement

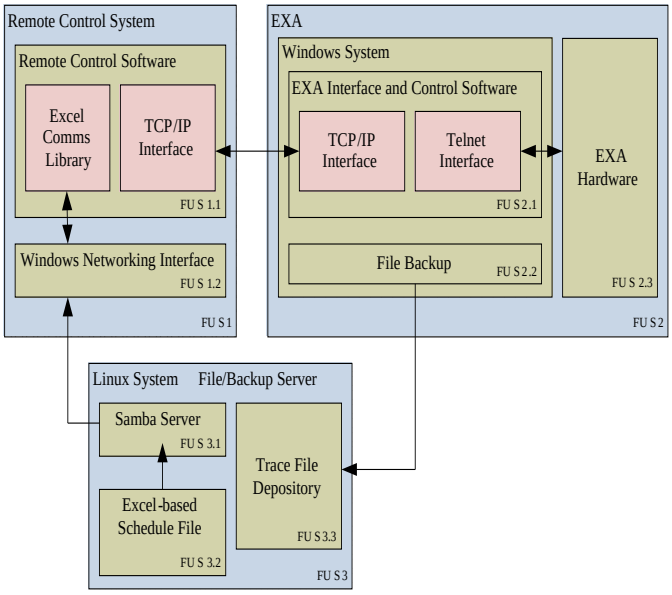

Figure 3: Software component functional block diagram of spectrum sensing system.

schedule file (hosted on a secure data storage server, FU H4) and for sending relevant configuration commands and requests to the SA, FU H2.4. The file backup software sporadically checks the local storage location for new data and then moves them to the data storage server, FU H4.

2.3. System calibration and sensitivity

The major functional components of the measurement system have all been calibrated using an Agilent E5071C ENA series network analyser. Fig. 4 illustrates the complete system link budget and includes the calibrated gains for the antenna G_a, the coaxial cables (LMR 600, G_{cl}, and Sucoflex 100, G_{cs}) and the LNA G_{lna}.

The total calibrated gain of the system G_{tot}, illustrated by the red line in Fig. 4, is a linear combination of the gain curves of all the major physical elements of the system and may thus be calculated as follows,

$$G_{tot} = G_a + G_{cl} + G_{cs} + G_{lna}. \quad (1)$$

The receiver sensitivity of the system S_r was also calculated to assist in determining the detection threshold λ_T. This was calculated by subtracting the total calibrated

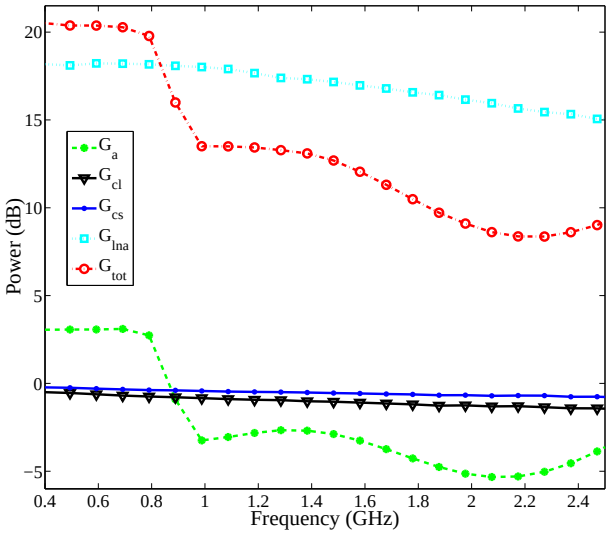

Figure 4: Link budget of hardware setup.

gain G_{tot} of the system from the received signal $r(n)$ as follows,

$$S_r = r\,(n) - G_{tot}. \tag{2}$$

2.4. Measurement description and schedule

During the measurement campaign, six week's worth of data were collected using the energy detection technique [17]. A measurement schedule was developed so as to maximise the number of samples that may be recorded over a period of time. Consecutive measurements were thus taken daily, spaced at two hourly intervals. During each scan, 1500 sweeps over the band of interest were completed. Each sweep sampled a number of points relating to the typical resolution of the channels being used in that band. Since channels in the GSM bands are traditionally spaced 200 kHz apart, the sampling resolution was set at 100 kHz. The UHF band is typically used for terrestrial television broadcasting, in South Africa, with a channel bandwidth of 8 MHz. The resolution of this band was thus set at 2 MHz. The bands measured, as well as the employed measurement band resolution, are listed in Table 1.

Description	Band (MHz)	Resolution (kHz)
UHF	470 - 854	2000
GSM900 DL	935 - 960	100
GSM1800 DL	1805 - 1880	100

Table 1: Spectrum measurement band descriptions

3. Spectrum occupancy

To calculate spectrum occupancy it is necessary to separate the information carrying component of a measured signal from its noise component. In this section the method employed for this purpose is described.

3.1. Signal detection

As previously mentioned, the energy detection method was selected to capture activity on the measured bands. Energy detection is one of the most commonly implemented approaches to spectrum sensing in CR applications. Signal detection is performed by comparing the output of an energy detector to a predetermined threshold. This threshold is influenced by the environmental noise floor. Mathematically, the detected signal may be represented by the following signal model [17],

$$r\,(x) = s\,(x) + w\,(x)\,, \tag{3}$$

where $s\,(x)$ is the transmitted signal and $w\,(x)$ denotes additive white Gaussian noise (AWGN). If one assumes that channel occupancy follows a binary model of being either unoccupied H_0 or occupied H_1, then the following binary hypothesis may be formulated,

$$r\,(x) = \begin{cases} w\,(x)\,, & H_0 \\ s\,(x) + w\,(x)\,, & H_1 \end{cases} \tag{4}$$

To test this binary hypothesis a signal detection threshold λ needs to be calculated under noise only conditions. A decision metric Y may then be compared against this threshold to determine channel occupancy [18].

Signal detection performance may be defined in terms of the probability of detection P_d and the probability of false alarm P_{fa} [19]. These probabilities are also known as the receiver operating characteristics (ROC). Apart from P_d, the measured signal may suffer from another type of

error, namely the probability miss-detection P_{md}, which is given as, $P_{md} = 1 - P_d$. It is desirable for both P_{fa} and P_{md} to be minimised. These erroneous conditions are defined as follows [20]: the miss-detection probability is the probability of detecting the band of interest to be free when it is actually already occupied,

$$P_{md} = P\{Y = H_0|H_1\} = P\{Y \leq \lambda|H_1\} \tag{5}$$

and the probability of false alarm is the probability of detecting a channel to be occupied by a PU when the PU is not actually present.

$$P_{fa} = P\{Y = H_1|H_0\} = P\{Y > \lambda|H_0\} \tag{6}$$

3.2. Threshold calculation

The detection threshold λ needs to be calculated so as to allow for the binary hypothesis, described in (4), to be tested. A threshold detection method that relies on the statistical properties of $r(x)$, has been proposed in the literature [21]. This method is known as the recursive one-sided hypothesis test (ROHT) and makes the assumption that the noise component of the signal with always follow a Gaussian distribution.

In this section a new method, inspired by the ROHT method, is proposed by the authors. This method is described as the maximum normal fit (MNF) method. For the MNF method, the assumption is made, as with the ROHT method, that the noise component of $r(x)$ is represented by the lowest set of samples in the distribution and that it follows a Gaussian distribution. However, in contrast to the ROHT method, the MNF method does not require that the distribution of the signal component of (3) be specifically defined. Furthermore, the MNF method follows a 'best-fit' approach to calculating the noise threshold, as opposed to the 'recursive-removal' approach followed by the ROHT method [21]. In the MNF method the statistical distribution of the signal and noise components is estimated and the point where they intersect is computed as the detection threshold.

3.2.1. Maximum normal fit algorithm

The probability density function (PDF) of the received signal, $r(x)$, can be described by the following expression,

$$\begin{aligned} f_R(x, \alpha, \mu, \sigma) = & f_{R_N}(x, \alpha_N, \mu_N, \sigma_N) \quad + \\ & f_{R_S}(x, \alpha_S, \mu_S, \sigma_S), \end{aligned} \tag{7}$$

where α is the amplitude, μ the mean and σ the standard deviation of the combined distribution. The PDFs of the noise and signal components of (7) can be defined by f_{R_N} and f_{R_S} respectively, and are assumed to follow a Gaussian distribution.

The MNF algorithm commences by attempting to isolate the peak values of this distribution by computing the roots of (7). These roots are calculated by determining where the approximate gradient of (7) is equal to zero,

$$\frac{df_R(x, \alpha, \mu, \sigma)}{dx} = 0. \tag{8}$$

The approximate gradient is computed by calculating the differences between the adjacent elements of (7).

The first root is assumed to represent the peak value P_N of the noise component and the second root, the peak value P_S of the signal component of (7). The sample at the first root is used to estimate the mean μ_N of the noise distribution and the sample at the second root to estimate the mean μ_S of the signal distribution. The MNF algorithm continues by isolating the noise component of (7) by using P_N; the first half of the noise distribution is found by taking all the samples from the lowest sample up to the sample containing P_N. The second half of the distribution is found by mirroring the first half, resulting in the following distribution,

$$f_{R_N}(x, \alpha_N, \mu_N, \sigma_N) = \frac{\alpha_N}{\sqrt{(2\pi\sigma_N^2)}} e^{-\frac{1}{2}\left(\frac{x-\mu_N}{\sigma_N}\right)^2}. \tag{9}$$

The amplitude term α_N in (9), is assumed to be P_N. The initial standard deviation $\hat{\sigma_N}$ and amplitude $\hat{\alpha_N}$ of the estimated noise distribution are randomly guessed (within arbitrary selected minimum bounds) and compared to the

isolated noise component (7), as follows,

$$\Delta f(x,\alpha,\mu,\sigma) = f_{R_N}(x,\alpha_N,\mu_N,\sigma_N) \quad - \quad f_N(x,\hat{\alpha_N},\hat{\mu_N},\hat{\sigma_N}), \tag{10}$$

where, f_N is the estimated noise distribution as described by the following expression,

$$f_N(x,\hat{\alpha_N},\hat{\mu_N},\hat{\sigma_N}) = \frac{\hat{\alpha_N}}{\sqrt{(2\pi\hat{\sigma_N^2})}} e^{-\frac{1}{2}\left(\frac{x-\hat{\mu_N}}{\hat{\sigma_N}}\right)^2}. \tag{11}$$

If the maximum difference in (10) for any value of x is not sufficiently small, then the standard deviation $\hat{\sigma_N}$ and amplitude $\hat{\alpha_N}$ are increased (the size of the increase and minimum bound leads to a trade-off between the convergence time and the accuracy of the algorithm). This process is continued until this difference becomes sufficiently small, such that,

$$max|\Delta f(x,\alpha,\mu,\sigma)| < \epsilon, \tag{12}$$

where ϵ represents an arbitrary small value, e.g. $\epsilon = 10^{-3}$. At this point, the values for $\hat{\sigma_N}$ and $\hat{\alpha_N}$ are taken to be the mean and standard deviation of the final estimate of the noise distribution.

The signal component f_{R_S} is then isolated from f_R by subtracting the noise distribution estimate f_N from f_R as follows,

$$f_{R_S}(x,\alpha_S,\mu_S,\sigma_S) = f_R(x,\alpha,\mu,\sigma) \quad - \quad f_N(x,\hat{\alpha_N},\hat{\mu_N},\hat{\sigma_N}). \tag{13}$$

Once estimates for the amplitude, mean and standard deviation of the noise distribution have been calculated, the estimated signal distribution $f_S(x,\hat{\alpha_S},\hat{\mu_S},\hat{\sigma_S})$ is obtained by repeating the same procedure as described from (9) to (12). From this process, estimates for the amplitude $\hat{\alpha_S}$, mean $\hat{\mu_S}$ and standard deviation $\hat{\sigma_S}$ of the signal distribution, are obtained. Hence, the intersection of the two estimated PDFs (f_N and f_S) is computed as follows,

$$f_N(x,\hat{\alpha_N},\hat{\mu_N},\hat{\sigma_N}) - f_S(x,\hat{\alpha_S},\hat{\mu_S},\hat{\sigma_S}) = 0. \tag{14}$$

The roots of (14) represent the detection threshold λ.

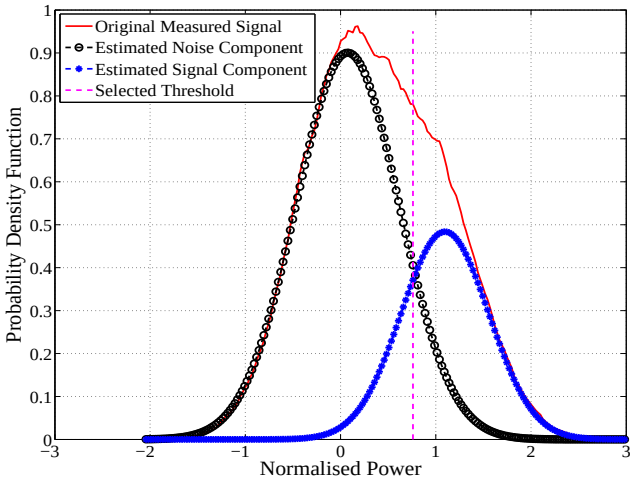

Figure 5: PDFs for the MNF method applied to a 40% occupied frequency band for data with an SNR of 3 dB.

3.2.2. Validation

Simulations were run to determine the best method to employ for calculating channel occupancy. The same approach and dataset was used when comparing the ROHT method to the MNF method. The approach followed, was to apply both methods to a specific time instant and spectrum segment, due to the fact that noise and signal statistics may vary over time and frequency, e.g., due to varying transmit power levels and fading of the channels over time. This results in a vector of noise thresholds, i.e., one value for each time instant and spectrum segment pair (each consisting of different noise and signal statistics).

The MNF method, applied to a channel that was simulated to be 40% occupied with a SNR of 3 dB, is illustrated in Fig. 5. Both the PDFs of the noise and of the signal were identified, and the threshold was calculated to be 0.7604 (in terms of normalized power). This resulted in an error of about 9.82%. The application of the ROHT method to the same data set, illustrated in Fig. 6, resulted in the threshold being calculated as 1.608 (in terms of normalized power) and ultimately lead to an error of 88.64%.

In Table 2, the MNF method is shown to also greatly outperform the ROHT method in other spectrum occu-

Table 2: The percentile error in occupancy when making use of the MNF and ROHT methods at SNR = 3 dB.

	MNF (3 dB)	**ROHT (3 dB)**
20	11.74	65.23
40	9.82	88.64
60	2.27	96.18
80	1.80	99.21
Occ. (%)	**Error (%)**	

pancy scenarios. The MNF method is not only significantly more accurate than the ROHT method, but it is also more versatile since no assumptions about the distribution of the signal component of (3) are required. Compared to the ROHT method, these advantages make the MNF method the preferred solution. The performance of the MNF algorithm can also be related to P_{fa} and P_{md}. If the calculated PDFs for both the noise and signal components of (3) are assumed to be fairly accurate, then the area under both curves should represent the sum of P_{fa} and P_{md}. Furthermore, there exists a point, under the two curves, where the area to the left (missed-detection) equals the area to the right (false-alarm). If this point is chosen as the threshold λ, then theoretically the same number of signal-samples will be missed as would be falsely identified. This would be the ideal solution for λ from a

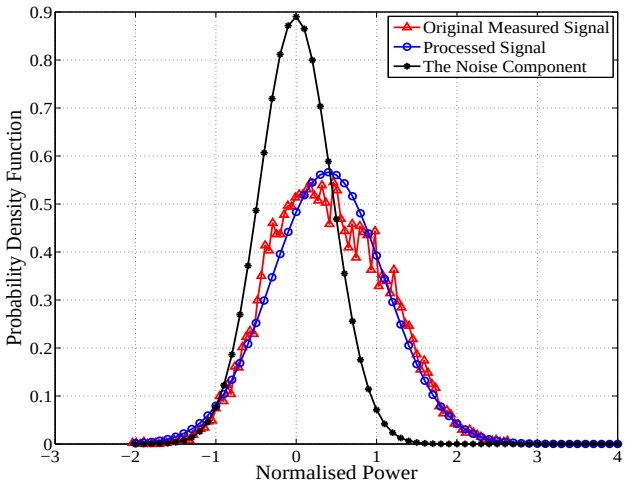

Figure 6: PDFs for the ROHT method applied to a 40% occupied frequency band for data with an SNR of 3 dB.

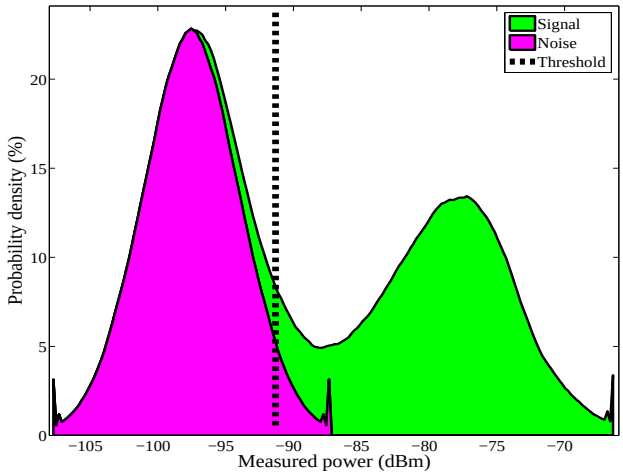

Figure 7: Statistical distribution of measured data indicating the level of the occupancy detection threshold for the GSM 900 band.

channel-occupancy perspective.

A graphical depiction of this process (for an instantaneous sample of the data that was measured in the GSM 900 MHz band) is illustrated in Fig. 7. The PDF to the left (coloured in purple) is assumed to represent the noise component of (3) and the PDF to the right (coloured in green) is assumed to represent the signal component of (3). The threshold λ, calculated using the MNF method, is indicated by the dotted black line.

3.3. Occupancy calculation

The occupancy of the bands measured was determined firstly by, calculating the value of λ and then by determining which of those measurements have actually exceeded λ. The individual measurements that exceed the threshold are then counted and divided by the total number of individual measurements ψ performed (for a particular band, k), so as to calculate the percentage occupancy of that band. Occupancy $O(k)$ was thus calculated according the following expression,

$$O(k) = 100\frac{\sum_{n=1}^{\psi}\rho(n,k)}{\psi}, \tag{15}$$

where,

$$\rho(n,k) = \begin{cases} 1, & r(n,k) > \lambda \\ 0, & r(n,k) \leq \lambda. \end{cases} \tag{16}$$

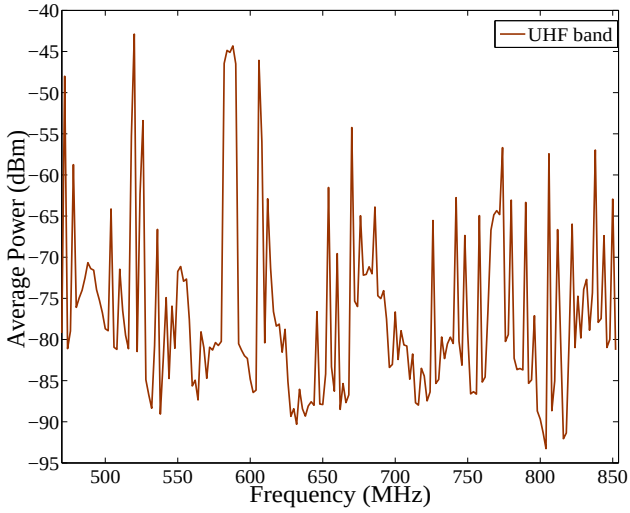

Figure 8: Average measured power of the UHF band.

4. Results

Presented here are results obtained from the processing of measurements from the UHF, GSM 900 down-link and GSM 1800 down-link bands [1]. All measured powers are presented in dBm and occupancies as a percentage of the total number of individual measurements performed. The data has been organised so as to show how the occupancy of the measured bands varies according to the time of day as well as the days of the week. The plots presented in this section were compiled by averaging the measurements taken over the course of the measurement campaign.

4.1. UHF bands

In light of the impending switch over from analogue to digital television in South Africa, measurements were taken from the UHF bands to gain greater insight into their utilisation. A similar heat map that shows the average measured power of the UHF band over the course of an average week, is presented in Fig. 10. The average percentage occupancy over the course of the week is also provided. A plot of the average measured power across

[1]For the GSM bands only the down-link has been presented due to insufficient sensitivity of the measurement system to accurately measure activity in the up-link.

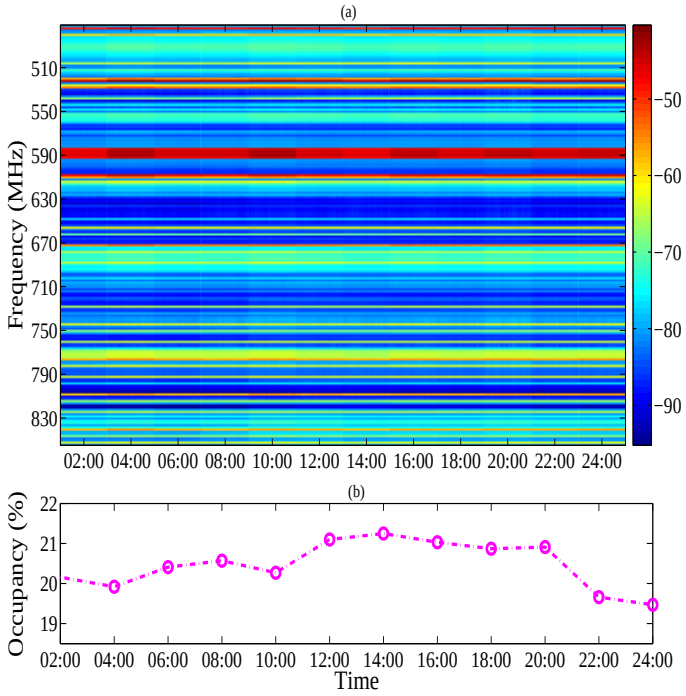

Figure 9: Heat map of the measured power of the UHF band over the course of an average day, part (a), and the associated percentage occupancy, part (b).

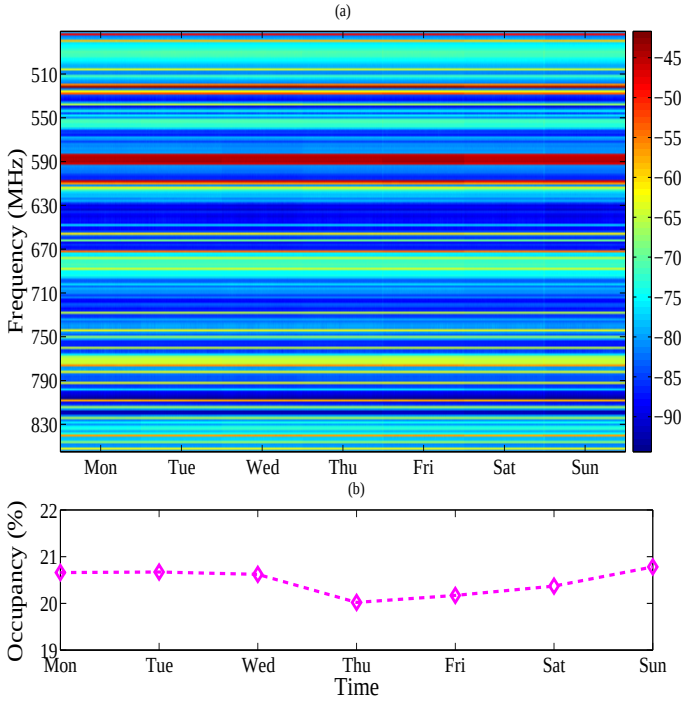

Figure 10: Heat map of the measured power of the UHF band over the course of an average week, part (a), and the associated percentage occupancy, part (b).

the range of UHF frequencies (470 MHz - 854 MHz) is presented in Fig. 8. A heat map of the average measured power of the UHF bands, over the course of an average day, is presented in Fig. 9. The average percentage occupancy over the same period is also provided.

From these plots, it is evident that although a number of strong signal components were present in the UHF band, it was found to be fairly underutilised at approximately only 20%. It was also clearly evident that there was very little fluctuation in the occupancy of this band over time. The lack of variation in occupancy was, however, to be expected as this band is primarily used for broadcast television. The low occupancy of this band is indicative of the relatively small number of terrestrial television stations available to South African viewers and the opportunity for better utilisation thereof.

4.2. GSM 900 MHz bands

A plot of the average measured power, across the GSM 900 MHz range of down-link frequencies, is presented in Fig. 11. It is immediately evident that there appears to be a significant amount of activity in these bands.

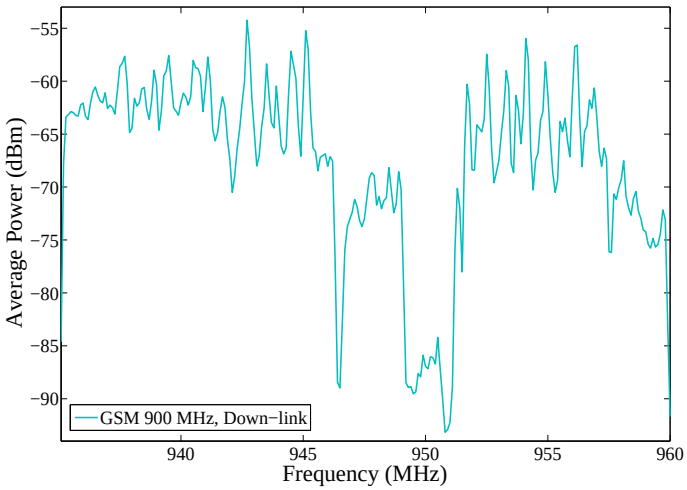

Figure 11: Average measured power of the down-link of the GSM 900 MHz band.

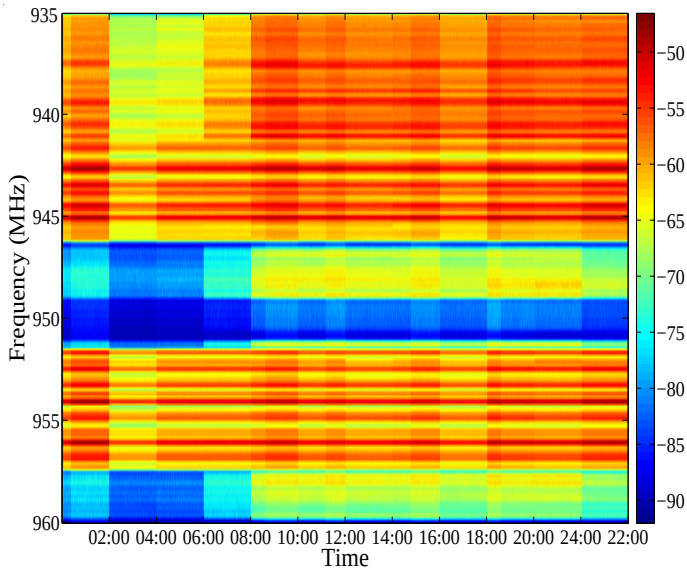

Figure 12: Heat map of the measured power of the down-link of the GSM 900 MHz band over the course of an average day.

4.2.1. Hourly occupancy

In Fig. 12, a heat map of the average measured power of the GSM 900 MHz down-link bands is presented. The corresponding percentage occupancy of these bands is provided in Fig. 13. It is immediately evident that the occupancy of both bands fluctuates over the course of the day.

From Fig. 13, it may be deduced that activity within the GSM 900 MHz bands appears to be at its lowest between

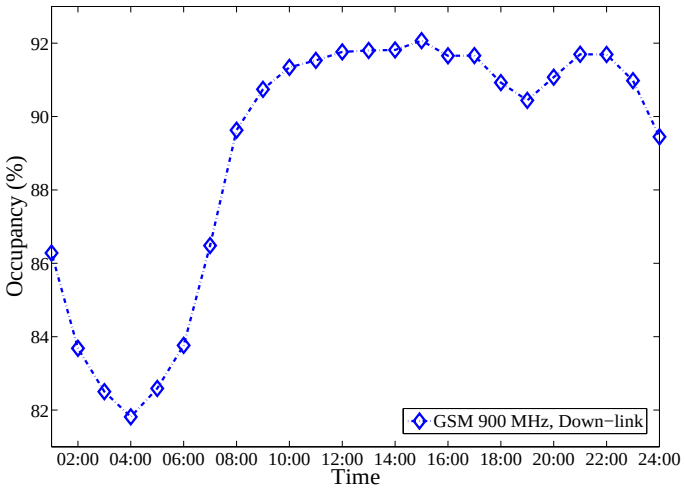

Figure 13: Percentage occupancy of the down-link of the GSM 900 MHz band over the course of an average day.

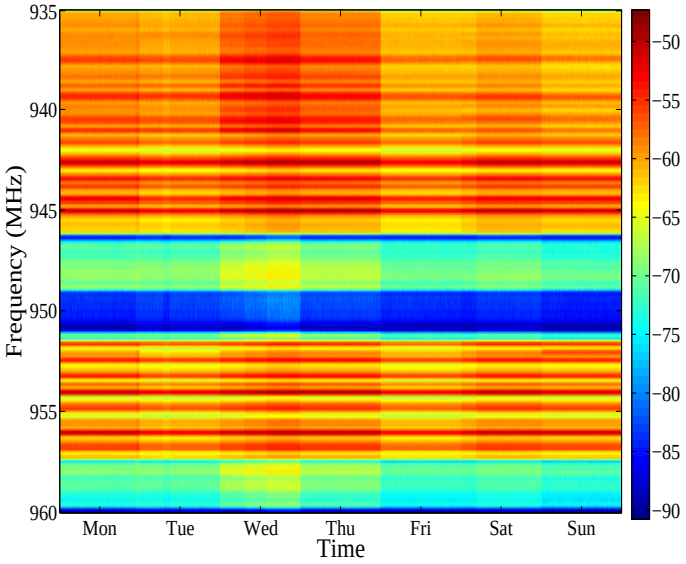

Figure 14: Heat map of the measured power of the down-link of the GSM 900 MHz band over the course of an average week.

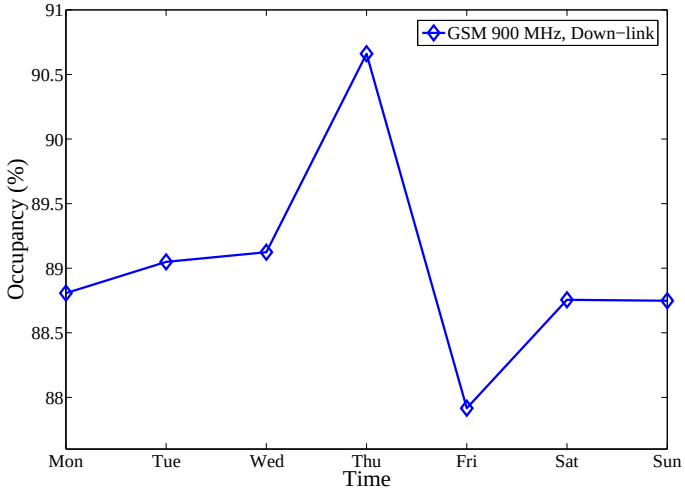

Figure 15: Percentage occupancy of the down-link of the GSM 900 MHz band over the course of an average week.

00:00 and 07:00, dropping to roughly 82% after which occupancy then increases to 92% by 10:00. Occupancy then remains relatively constant until approximately 22:00 after which it begins to steadily drop until 04:00 the following morning. This pattern is not surprising, as occupancy seems to be low when mobile users are likely to be sleeping and high when they are likely to be involved in business or work activities.

4.2.2. Daily occupancy

In Fig. 14, a day-to-day heat map of the average measured power of the GSM 900 MHz up-link bands is presented. The corresponding percentage occupancy is illustrated in Fig. 15. Occupancy over the course of the week appears to be fairly constant with a fluctuation of approximately only 1% between week days and weekends. However, it is interesting to note that there seems to be a small spike in activity of around 2% on Thursdays before the slight drop in activity over the weekends.

4.3. GSM 1800 MHz bands

A plot of the average measured power across the GSM 1800 MHz range of frequencies is presented in Fig. 16.

4.3.1. Hourly occupancy

In Fig. 17, a heat map of the average measured power of the GSM 1800 MHz down-link bands is presented. The corresponding percentage occupancy of these bands is illustrated in Fig. 18. Similar trends with regard to hourly occupancy in the GSM 900 MHz bands are observable in the GSM 1800 MHz bands. The main difference being that the GSM 1800 MHz band was found to be less than half as occupied as its GSM 900 MHz counterpart (from 20% to 40% occupied compared to 80% to 90%).

In Fig. 18, it appears that the first and last 10 MHz, of

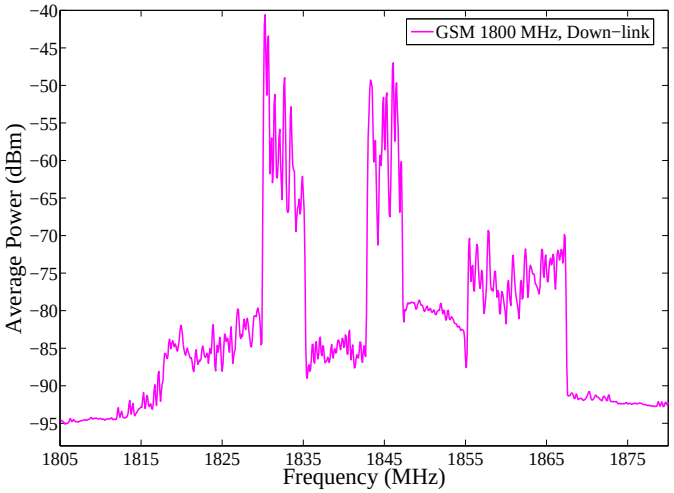

Figure 16: Average measured power of the down-link of the GSM 1800 MHz band.

both the up-link and down-link portions of the GSM 1800 MHz bands are completely unoccupied. It is possible that the considerably lower occupancy of the GSM 1800 MHz may be partly explained by this observation.

4.3.2. Daily occupancy

In Fig. 19, a day-to-day heat map of the average measured power of the GSM 1800 MHz down-link bands is presented. The corresponding percentage occupancy is illustrated in Fig. 20. Similar trends with regard to hourly occupancy in the GSM 900 MHz bands are again observable in the GSM 1800 MHz bands. From Fig. 20, it can be seen that the occupancy of the GSM 1800 MHz band from day-to-day also exhibits fairly low fluctuation. However, the difference between week day and week end occupancy does seem to be more clearly defined than in the measurements from the GSM 900 MHz bands, particularly for the down-link bands, where on average a difference of approximately 5% is visible between Thursdays and Saturdays.

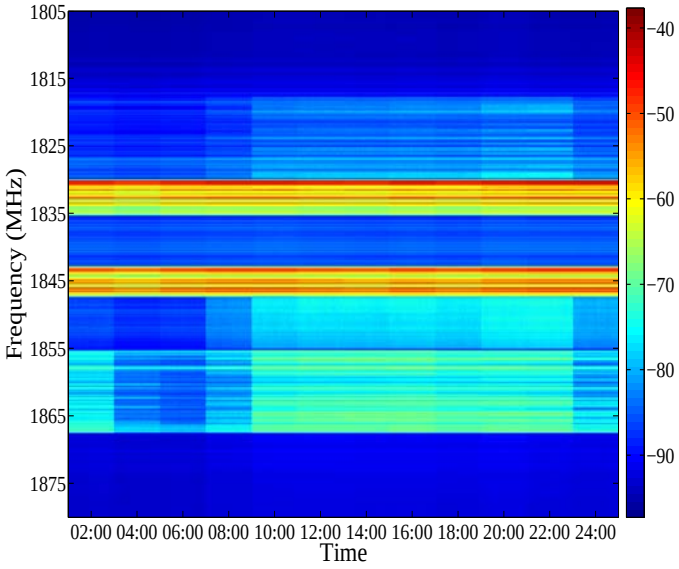

Figure 17: Heat map of the measured power of the down-link of the GSM 1800 MHz band over the course of an average day.

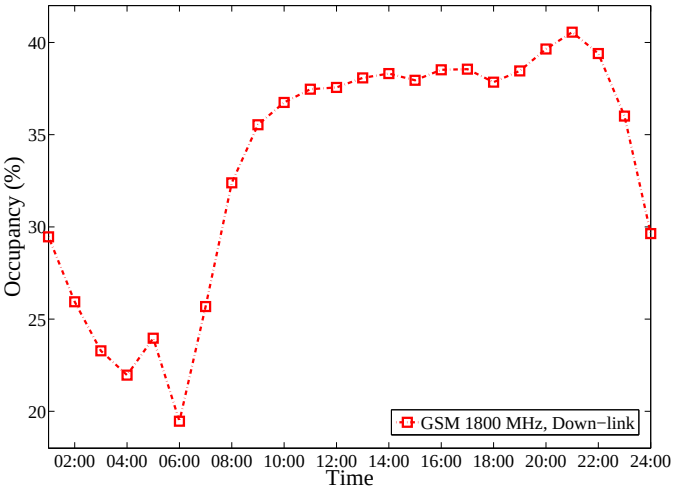

Figure 18: Percentage occupancy of the down-link of the GSM 1800 MHz band over the course of an average day.

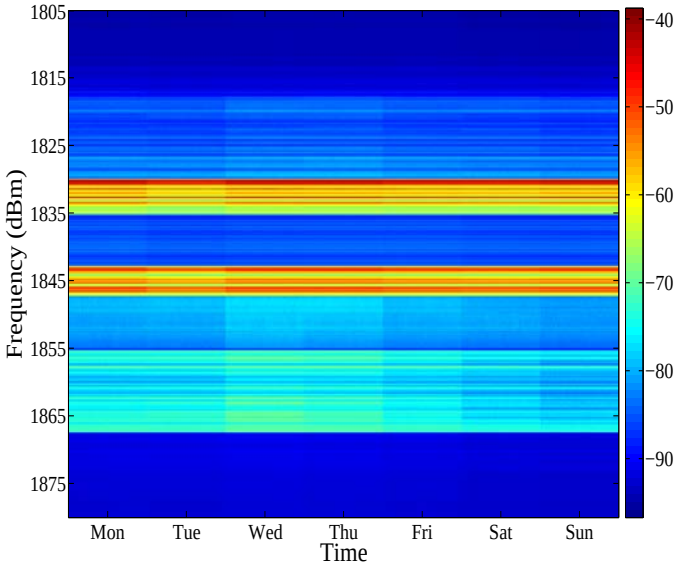

Figure 19: Heat map of the measured power of the down-link of the GSM 1800 MHz band over the course of an average week.

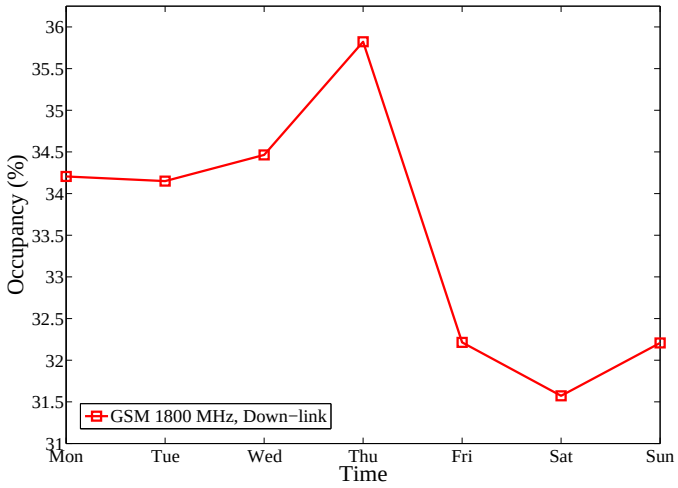

Figure 20: Percentage occupancy of the down-link of the GSM 1800 MHz band over the course of an average week.

5. Comparative analysis

In Table 3, a brief comparison is made between the results obtained from this measurement campaign, and those obtained from various measurement campaigns in other cities around the world. A comparison is made against the reported average occupancy of bands used for television broadcasting as well as those used for mobile cellular communications in Chicago, Vienna (Virginia) and Dublin (Ireland) [5, 10, 6]. The values presented in Table 3 have thus been calculated as a percentage of the average occupancy of the bandwidth allocated for either broadcast television or mobile communication at the measurement location in question. Mobile A refers to the bands allocated for cellular communication around the 800/900 MHz region and mobile B refers to those around the 1800/1900 MHz region.

Table 3: A brief comparison of the measured average percentage spectrum occupancy in various cities around the world.

Band	**Pretoria**	**Chicago**	**Vienna**	**Dublin**
TV	20	65	37	18
Mobile A	89	60	45	1
Mobile B	33	20	16	34

Certain observations can be made from Table 3. Firstly, that the broadcast TV channels in Pretoria and Dublin are much less occupied than their American counterparts, secondly, that the mobile bands seem to be more heavily utilised in Pretoria than at the other locations (particularly for mobile A) and thirdly, that mobile A appears to have a higher percentage occupancy than mobile B (with the exception of Dublin, Ireland).

It must be noted that regulatory policy surrounding frequency planning differs amongst these locations. It is thus difficult to obtain an exact comparison of occupancy, since there are differences in the bandwidths set aside for mobile communication for each country and in the number TV stations operating at each location. However, it is clear that there is still available spectrum in the TV and cellular bands, that could be exploited by more spectrally efficient technologies such as cognitive radio.

6. Conclusion

A spectrum measurement system was developed and measurements were taken in attempt to gather more information about the utilisation of certain commercially utilised frequency bands in South Africa. As a case study, detailed measurements were taken from the South African UHF, GSM 900 MHz and GSM 1800 MHz bands in the Hatfield area of Pretoria, South Africa.

The authors presented the MNF method, which was developed as a technique for extracting the information bearing component from the noise component of a measured signal, and it was shown that it outperformed the existing ROHT method. The MNF method was thus used to calculate spectrum occupancy.

Results indicate that spectrum occupancy remains fairly constant for the UHF bands at approximately only 20%. While the maximum occupancy of the GSM 900 MHz band was calculated to be much higher at approximately 92% and that of the GSM 1800 band to be approximately 40%. However, the GSM 900 MHz and 1800 MHz bands did exhibit fluctuations in occupancy of between 10% and 20% respectively according to the time of day. Slight variations of between 1% and 3% were also evident over the days of the week.

A comparison against the findings of other spectrum occupancy studies around the world shows varying degrees of occupancy for the TV and cellular bands but does, however, indicate that there is available spectrum that could be exploited by more spectrally efficient technologies, such as cognitive radio.

Further measurement campaigns, across other parts of the country, would be beneficial to the regulatory body.

7. Acknowledgement

This research is supported by the Sentech Chair in Broadband Wireless Multimedia Communication (BWMC), the National Research Foundation (NRF) and the Independent Communications Authority of South Africa (ICASA). The authors would also like to thank Mr M.J. Prinsloo for his contribution.

References

[1] Federal Communications Commission, Spectrum policy task force report, Tech. Rep. ET Docket 02-155 (Nov. 2002).

[2] T. A. Weiss, F. K. Jondral, Spectrum pooling: an innovative strategy for the enhancement of spectrum efficiency, IEEE Commun. Mag. 42 (3) (2004) 8–14.

[3] J. Mitola III, G. Q. Maguire Jr., Cognitive radio: making software radios more personal, IEEE Pers. Commun. 6 (4) (1999) 13–18.

[4] S. D. Barnes, B. T. Maharaj, Performance of a hidden Markov channel occupancy model for cognitive radio, in: Proc. IEEE AFRICON Conf., Livingstone, Zambia, 2011, pp. 1–6.

[5] T. M. Taher, R. B. Bacchus, K. J. Zdunek, D. A. Roberson, Long-term spectral occupancy findings in Chicago, in: Proc. IEEE Int. Symp. Dynamic Spectr. Access Netw., Aachen, Germany, 2011, pp. 100–107.

[6] R. I. C. Chiang, G. B. Rowe, K. W. Sowerby, A quantitative analysis of spectral occupancy measurements for cognitive radio, in: Proc. IEEE Veh. Technol. Conf., Dublin, Ireland, 2007, pp. 3016–3020.

[7] M. Lopez-Benitez, F. Casadevall, R. Hachemani, J. Palicot, Spectral occupation measurements and blind standard recognition sensor for cognitive radio networks, in: Proceedings of the Fourth International Conference on Cognitive Radio Oriented Wireless Networks and Communications, Hannover, Germany, 2009, pp. 1–9.

[8] M. Matinmikko, M. Mustonen, M. Höyhtyä, T. Rauma, H. Sarvanko, A. Mämmelä, Distributed and directional spectrum occupancy measurements in the 2.4 GHz ISM band, in: Proc. Int. Symp. Wireless Commun. Syst., York, United Kingdom, 2010, pp. 976–980.

[9] M. A. McHenry, NSF spectrum occupancy measurements project summary, Tech. rep., Shared Spectrum Company (Aug. 2005).

[10] M. A. McHenry, D. McClokey, D. Roberson, J. T. MacDonald, Spectrum occupancy measurements Chicago Illinois, Tech. rep., Shared Spectrum Company, Vienna, Virginia (Nov. 2005).

[11] M. A. McHenry, P. A. Tenhula, D. McCloskey, D. A. Roberson, C. S. Hood, Chicago spectrum occupancy measurements & analysis and a long-term studies proposal, in: Proc. Int. Workshop Technol. Policy Accessing Spectr., Boston, MA, 2006.

[12] M. Wellens, J. Wu, P. Mähönen, Evaluation of spectrum occupancy in indoor and outdoor scenario in the context of cognitive radio, in: Proc. 2nd Int. Conf. Cognitive Radio Oriented Wireless Netw. Commun., Orlando, FL, 2007, pp. 420–427.

[13] M. Wellens, A. de Baynast, P. Mähönen, Performance of dynamic spectrum access based on spectrum occupancy statistics, IET Commun. 2 (6) (2008) 772–782.

[14] M. Wellens, J. Wu, P. Mähönen, Lessons learned from an extensive occupancy measurement campaign and stochastic duty cycle, Mobile Netw. Appl. 15 (3) (2010) 461–474.

[15] S. D. Barnes, Cognitive radio performance optimisation through spectrum availability prediction, Master's thesis, University of Pretoria (2012).

[16] B. T. Maharaj, S. D. Barnes, Spectrum measurement and performance for cognitive radio, University of Pretoria, Pretoria, South Africa, 2012, iSBN 978-1-77592-021-2.

[17] T. Yücek, H. Arslan, A survey of spectrum sensing algorithms for cognitive radio applications, IEEE Commun. Surveys Tuts. 11 (1) (2009) 116–130.

[18] K. Kim, I. A. Akbar, K. K. Bae, J.-S. Um, C. M. Spooner, J. H. Reed, Cyclostationary approaches to signal detection and classification in cognitive radio, in: Proc. 2nd IEEE Int. Symp. New Frontiers Dynamic Spectr. Access Netw., Dublin, Ireland, 2007, pp. 212–215.

[19] C. Ghosh, C. Cordeiro, D. P. Agrawal, M. B. Rao, Markov chain existence and hidden markov models in spectrum sensing, in: Proc. 7th Annu. IEEE Int. Conf. Pervasive Comput. Commun., Galveston, TX, 2009, pp. 1–6.

[20] K. Dhuness, B. T. Maharaj, A cognitive radio application of OM-OFDM, in: Proc. IEEE AFRICON Conf., Livingston, Zambia, 2011, pp. 1–5.

[21] D. Datla, A. M. Wyglinski, G. J. Minden, A spectrum surveying framework for dynamic spectrum access networks, IEEE Trans. Veh. Technol. 58 (8) (2009) 4158–4168.